Ultrafast Nanostructuring Oxidation of Crystallized Intermetallic ZrAu at 25 °C

J.-Ch. Valmalette,*,† M. Isa,† M. Passard,‡ and M. Lomello-Tafin‡

Laboratoire Matériaux Microélectronique de Provence (L2MP), CNRS, UMR 6137, Université de Toulon-Var, B.P. 132, F-83957 La Garde Cedex, France, and Laboratoire d'Instrumentation et des Matériaux d'Annecy (LAIMAN), Université de Savoie, B.P. 240, F-74942 Annecy-Le-Vieux, France

Received July 19, 2001. Revised Manuscript Received November 30, 2001

In this study we first report the elaboration of gold and zirconia clusters (ranging from 3.5 to 7 nm in size) obtained by air oxidation of crystallized ZrAu at 25 °C within a few hours. This transformation was observed using X-ray diffraction, infrared spectroscopy (transmission and DRIFTS), and electron microscopy (SEM and HREM) techniques. This solid-state nanostructuration is interpreted as a consequence of combined mechanisms: adsorption and diffusion of oxygen, segregation of gold atoms from ZrAu alloy onto Au clusters, and acceleration of the process by internal residual stress and percolation of the electronic current via gold-cluster chains. The gaseous species adsorption by very small gold clusters supported by zirconia formed at the initial step of this oxidation could induce "catalytically assisted nanostructuring oxidation". Large amounts of gold and zirconia nanoparticles are obtained at the end of this process.

Introduction

Noble metal clusters dispersed in very fine metal oxide powders are being intensively studied since it has been shown that highly divided solids enhance many physical and chemical properties. These nanostructured materials show promising catalytic and nonlinear optical properties. Both physical and chemical methods are commonly used to obtain various sizes, shapes, orientations, and concentrations of noble metal clusters.[1−3] Currently, the elaboration of very small particles with a large volume fraction of noble metal through large-scale and low-cost processes remains an unresolved problem. In chemical methods involving thermal decomposition of precursors, the high temperature required for total transformation induces cluster growth at a high volume fraction of noble metal. While extensively used, coprecipitation of noble metal with a variety of metal oxides is also restricted to low concentrations of noble metals to avoid coalescence. At higher concentration levels, stabilization of clusters can be achieved by adsorption of large molecules, which modifies the surface properties. Chemical processes generally involve a liquid medium and/or thermal treatment, which, in turn, create cluster motion, coalescence, and growth. The oxidation of glassy ZrAu and ZrPd alloys[4−6] at a temperature above 300 °C has been shown to be an interesting method for obtaining high surface catalyst.

In this paper, we demonstrate that thermal treatment is not necessary to oxidize ZrAu alloys if they are crystallized. Indeed, we previously established a new version of the Zr−Au phase diagram showing the presence of eight crystallized intermetallic compounds and several solid-state transformations (allotropic, martensitic) occurring in the equiatomic region.[7] We indicated that the oxidation behavior of these crystallized Zr/Au alloys is related to the composition and microstructure, which depend on the synthesis conditions.[8] In contrast with the oxidation of amorphous Zr/Au alloys presented by Shibata et al., the oxidation of crystallized alloys in the equiatomic region starts at room temperature to form gold and zirconia nanoparticles.[9] The aim of this work was to investigate low-temperature synthesis of noble metal clusters mixed with solid-state metal oxide clusters. The high instability of crystallized ZrAu alloys is of great interest both for the synthesis of nanostructured materials[10] and for understanding an unusual oxidation mechanism.

* To whom correspondence should be addressed. E-mail: valmalette@univ-tln.fr.
† Université de Toulon-Var.
‡ Université de Savoie.

(1) Goia, D. V.; Matijevic, E. *Colloids Surf. A* **1999**, *146*, 139−142.
(2) Zhou, Y. C. Y, Zhu, Y. R., Chen, Z. Y. *Commun. Chem. Mater.* **1999**, *11* (9), 2310, 3.
(3) Goia, D. V.; Matijevic, E. *New J. Chem.* **1998**, *22* (11), 1203.
(4) Shibata, M.; Kawata, N.; Masumoto, T.; Kimura, H. *Chem. Lett.* **1985**, 1605−1608.
(5) Baiker, A.; Maciejewski, M.; Tagliaferri, S. *Ber. Bunsen-Ges. Phys. Chem.* **1993**, *97*, 3, 286−292.
(6) Baiker, A.; Maciejewski, M.; Tagliaferri, S.; Hug, P. *J. Catal.* **1995**, *151*, 407−419.
(7) Lomello-Tafin, M.; Galez, P.; Gachon, J. C.; Feshotte, P.; Jorda, J. L. *J. Alloys Compd.* **1997**, *257*, 215−223.
(8) Valmalette, J.-C.; Lomello-Tafin, M.; Galez, P.; Jorda, J.-L. Communication, 4th International Conference on Nanostructural Materials, NANO'98, Stockholm, Sweden, 1998.
(9) Valmalette, J.-C.; Isa, M.; Stadelmann, P.; Lomello-Tafin, M.; Passard, M.; Jorda, J.-L. Oral Communication, 5th International Conference on Nanostructural Materials, NANO'2000, Sendai, Japan, 2000.
(10) Lomello-Tafin, M.; Valmalette, J. C.; Jorda, J. L.; Galez, Ph. Patent FR-98 08343, 1998.

10.1021/cm011184z CCC: $22.00
Published on Web 04/03/2002

Experimental Section

Initial crystallized $Zr_{0.5}Au_{0.5}$ ingots were prepared by arc-melting under an Ar atmosphere from Zr and Au wires of 99.7% and 99.99% Au purity, respectively. The initial Zr:Au atomic ratio measured by X-ray emission analysis (EDAX) was found to be uniform and equal to 1.02 ± 0.07. These observations are consistent with the congruent formation of the equiatomic compound. Samples obtained are about 1 cm^3 and show metallic luster on the surface. Subsequently, ZrAu alloy ingots were cut into 1 mm thick slices using a diamond saw, mechanically polished, and placed in sealed quartz tubes under vacuum to prevent oxidation. Microstructural investigations were made after chemical etching of the surface in aqua regia for 20 s. Nanostructuration experiments on the samples were performed in air at a regulated temperature of 25 ± 2 °C with different relative humidities (65 ± 5% and 100% RH).

X-ray diffraction patterns were collected on a Siemens-Bruker D5000 diffractometer using Cu Kα radiation (35 mA, 45 kV) with a back monochromator over a 2θ range of 5−120° and a position-sensitive detector using a step of 0.01° and a step time ranging from 1 to 24 s according to the diffracted intensity. The mean crystallite sizes were estimated from reflections fitted by mixed Gaussian and Lorentzian functions. Investigations of the surfaces of the samples were performed using a Philips XL 30 scanning electron microscope operating with an accelerating voltage of 25 kV. As for the metallic samples, surface metallization of corroded slices was not necessary. EDAX was used to determine the elemental composition using standards and the classical ZAF corrections. High-resolution electron microscopic (HREM) investigations were carried out using a Philips EM 430 ST operating with an accelerating voltage of 300 kV with a LaB_6 source. Powders resulting from the oxidation reaction at the surfaces of the slices were dispersed by ultrasonic treatment in purified water. The complete nanostructuring oxidation of the ZrAu samples is achieved very rapidly in air and leads to the formation of ZrO_2 and gold. The powder obtained at the end of the process contains only Zr^{4+} and Au^0, and no further oxidation is expected during its dispersion in water. Suspensions were then dropped onto the carbon-coated copper grids and used for the investigations. The specific surface area measurements were made by nitrogen adsorption evaluated using a Brunauer−Emmett−Teller (BET) model with a Micromeritics Gemini 2375 instrument. Prior to the measurement, about 80 mg of powder resulting from the surface oxidation was dried under flowing nitrogen at 40 °C for 14 h and at 110 °C for 1 h to investigate the influence of temperature and time on the physisorption and possible cluster growth. S_{BET} values were calculated in a relative pressure range of $0.05 < p/p_0 < 0.3$ assuming a cross-section area of 0.162 nm^2 for the N_2 molecule. The FT-IR spectroscopy measurements were carried out with a Mattson-Nicolet RS spectrometer in transmission and diffuse reflectance modes (DRIFTS) in the 400−4000 cm^{-1} spectral range. Observations in the transmission mode were made by the classical KBr pellet technique, whereas DRIFTS measurements were performed on the surface of the sample submitted to oxidation.

Results

Micrographic observations of freshly prepared and chemically etched ZrAu samples show a characteristic martensitic microstructure with large and elongated grains, orientated in the same direction as illustrated in Figure 1a. The internal microstructure of these large grains shows very small and parallel domains (Figure 1b), which are also evidenced by their optical contrast (Figure 1c).

The visual aspect of the surfaces of the samples rapidly transforms within a few hours in air at room temperature, from metallic luster to dull black purple. After a few days, black pulverulent powder is projected

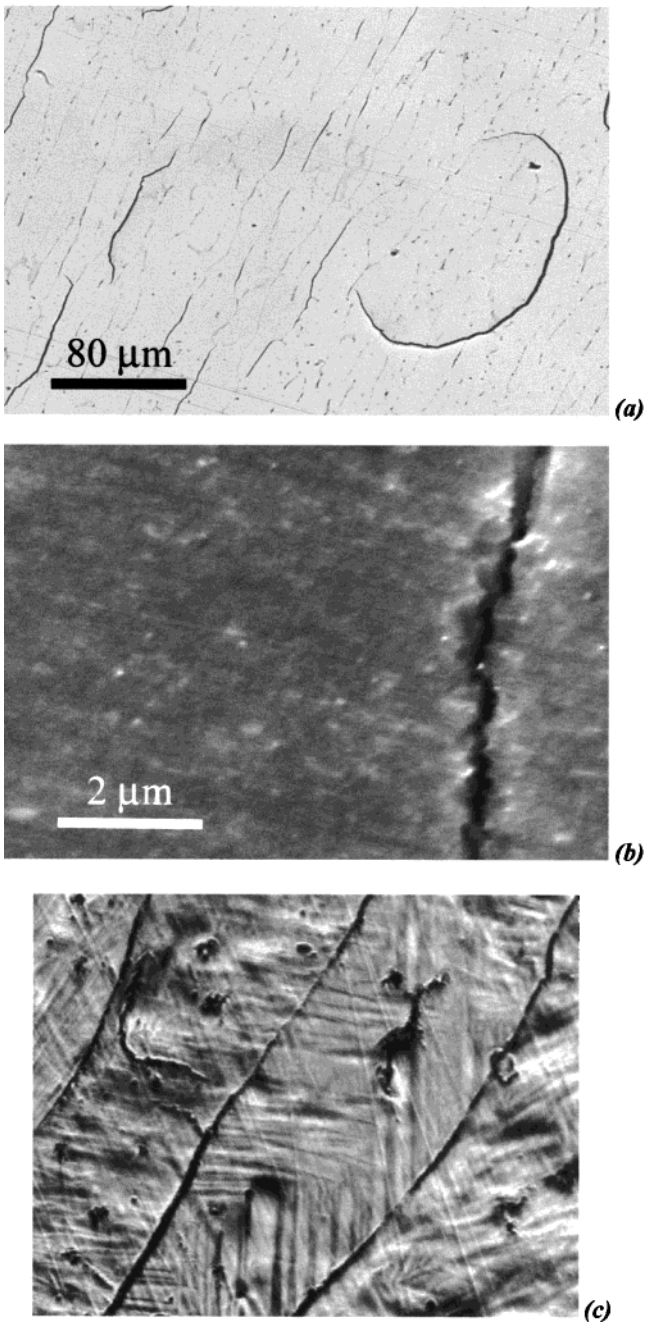

Figure 1. BSE micrograph of arc-melted ZrAu after etching in aqua regia (a), SE micrograph at higher magnification (b), and optical micrograph of 75 × 50 μm size (c).

around the sample. X-ray diffractograms of samples exposed in air at room temperature with 65 ± 5% RH show strong modifications after only a few hours (Figure 2). The relative intensity of all the diffraction peaks rapidly decreases, whereas new broad peaks appear. We should note here that the crystallographic structure of ZrAu is still unknown. However, the indexation of diffraction peaks with different structures of homologous intermetallics (ZrPd, ZrAg, and TiAu) suggests the presence of at least two crystallographic forms of ZrAu in the as-cast samples. The *d* spacing list and the related intensities, presented in Table 1, appear to be very similar for all samples analyzed, whereas the relative intensities tend to vary significantly. The rates of intensity decrease with oxidation (Figure 3) are not the same for all reflections: The first category (A), corresponding

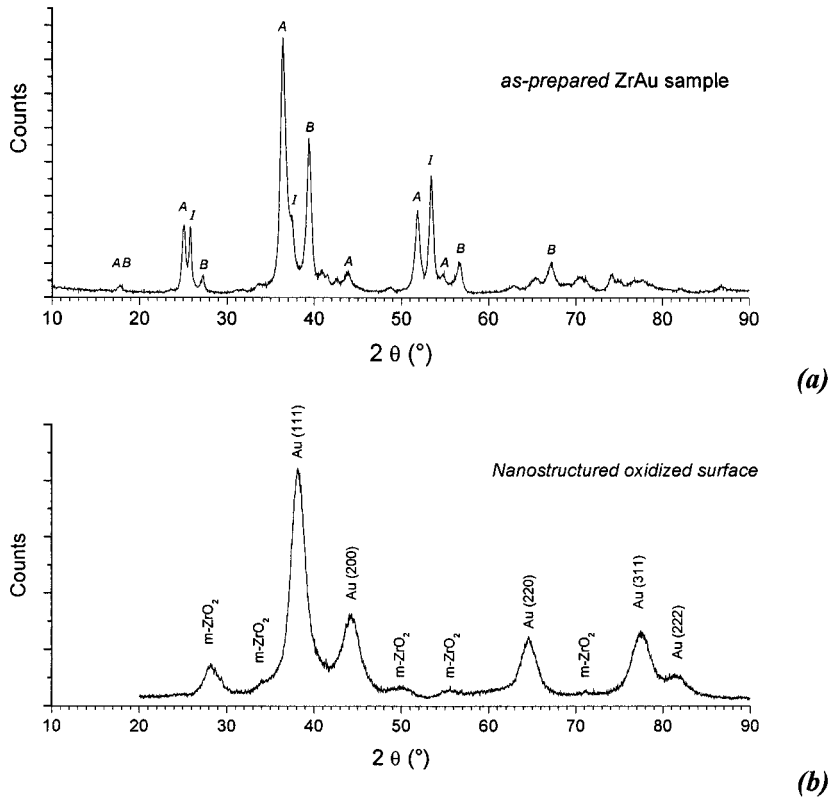

Figure 2. XRD pattern of freshly prepared ZrAu ingots (a) and after oxidation in air at 25 °C for 72 h (b).

Table 1. Experimental *d* Spacing and Intensities of As-Prepared ZrAu Samples

refln no.	*d* spacing (Å)	I_{exp}	refln no.	*d* spacing (Å)	I_{exp}
1	5.62	1	19	1.715	46
2	5.00	3	20	1.676	7
3	3.77	1	21	1.625	11
4	3.56	26	22	1.476	3
5	3.45	25	23	1.425	6
6	3.28	6	24	1.394	8
7	2.88	2	25	1.359	3
8	2.81	2	26	1.336	6
9	2.66	3	27	1.325	6
10	2.47	100	28	1.279	7
11	2.41	30	29	1.265	5
12	2.29	60	30	1.242	5
13	2.21	9	31	1.228	5
14	2.167	7	32	1.216	2
15	2.124	5	33	1.174	2
16	2.066	8	34	1.122	2
17	1.869	2	35	1.119	2
18	1.763	32			

to the peaks, shows a rapid evolution characterized by an onset time $t_{onset(A)}$ of about 14 h. The second category (B) corresponding to the peaks is characterized by a slower evolution with a $t_{onset(B)}$ of about 22 h. Finally, a few peaks show intermediate rates (category I).

After 40 h in air at 25 °C, all the initial reflections have totally disappeared and we observe five new broad peaks and modulations in the background. These peaks are attributed to the (111), (200), (220), (311), and (222) reflections of gold. Additional modulations could be assigned to the monoclinic ZrO_2, with the strongest peak at $2\theta = 28.30°$ associated with the (-111) reflection. Zirconia particle sizes estimated from XRD profiles and HREM images range from 4 to 8 nm. The estimated mean crystallite size of gold clusters formed during this transformation was estimated from (111), (200), (220),

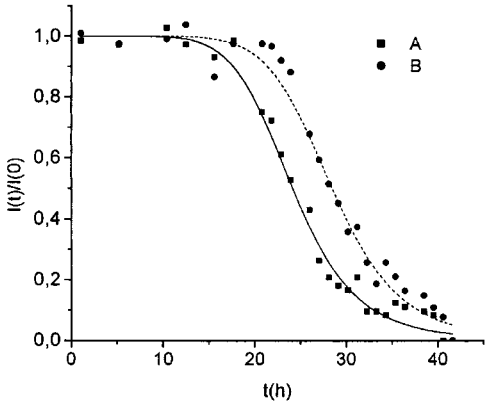

Figure 3. Evolution over time of the normalized intensity of diffraction peaks from category A and from the second category (B).

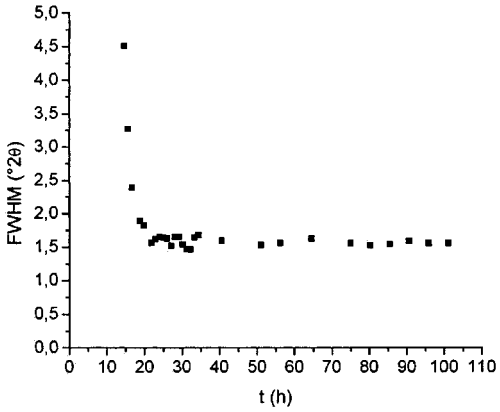

Figure 4. Evolution of the (111) Bragg reflection breadth of gold at 25 °C.

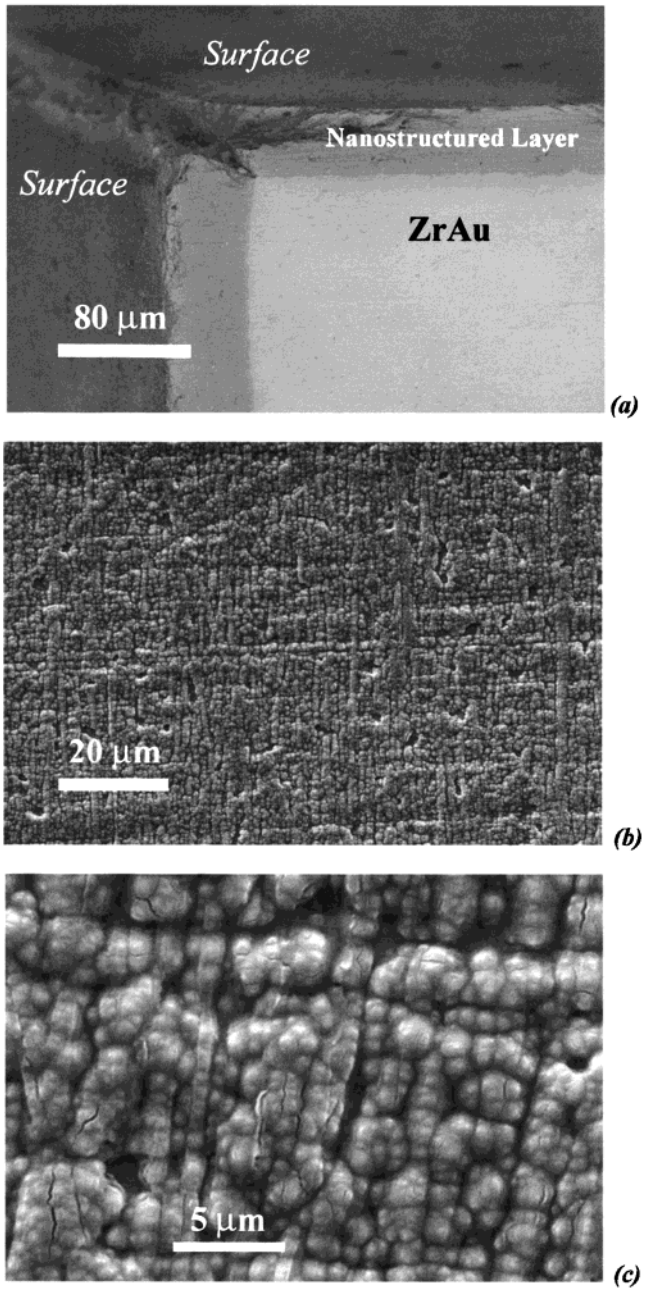

Figure 5. SEM micrographs of arc-melted ZrAu after oxidation for 10 days in an air laboratory: BSE image of the profile (a), SE image of the globular lined roughness of the surface (b), details in the SE mode of globules and cracks at the surface (c).

(311), and (222) reflections fitted by Pseudo−Voigt functions. The evolution of the peak profiles (Figure 4) over time indicates a significant cluster growth at the very beginning of the oxidation mechanism. Gold cluster growth is not linear over time: the initial growth is fast (3.5 nm in 24 h) and rapidly slows (7 nm after two years). Mechanical energy induced by manual milling in an agate mortar for a few seconds causes important crystal growth associated with the formation of reflecting gold coating of the surface of the mortar.

The surfaces of the samples exposed for 10 days in air at 25 °C with 65% RH were observed by electron microscopy. The BSE image in Figure 5a of the slice profile is represented as a side view. It reveals the formation of a continuous and homogeneous layer at the

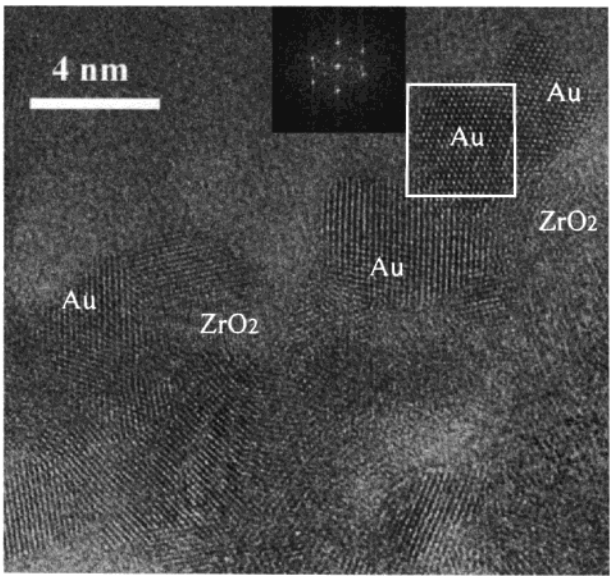

Figure 6. HREM of the nanostructured Au−ZrO_2 layer.

sample surface with lower density (light gray) than bulk ZrAu (dark gray). This contrast results from the presence of oxygen in this layer, confirmed by EDAX analyses. The concentrations of Zr, Au, and O are uniform in the light gray area and, respectively, equal to about 25, 25, and 50 atom % with variations lower than 2.7 atom %. With the spatial resolution allowed by this technique (about 1 μm), we cannot observe a concentration gradient that would correspond to a diffusion front. The interface between the oxidized layer and ZrAu is fairly linear and does not follow the contour of the large grains described in Figure 1a. The SE images of the surface represented in Figure 5b,c show a surprising globular lined roughness in two directions. The orientations have been shown to be independent of the polishing direction but related to the direction of the initial grain boundaries revealed by chemical etching (Figure 1a). At higher magnification, we can observe that each globule shows a crack on its surface.

After a few days, the nanostructured layer formed at the surface of the samples transforms into a black pulverulent powder, which is projected all around the sample. HREM images of this powder show a mixture of crystallized domains with sizes of about 4−6 nm (Figure 6). Analyses by EELS confirm the presence of two types of nanocrystals: gold and zirconia as indicated in the figure. This result closely matches the XRD experiments presented in Figure 2b. Domain sizes observed on HREM images are very similar to those deduced from the profile analyses of diffraction peaks. Identification of gold nanocrystals from HREM images was also made by FFT of selected areas. They correspond to the electron diffraction patterns of gold with the [1,1,0] zone axis. But a few gold clusters show additional spots (indicated in the square in Figure 6) which cannot be indexed in the fcc structure. Identification of monoclinic zirconia domains is not deduced from HREM images alone, because only one plane is observable in each area of these images, so correlation with HREM and EELS was used.

The infrared spectrum (Figure 7a) of the nanopowders analyzed in the transmission mode shows strong absorption bands at 498 and 577 cm^{-1} and a weaker one

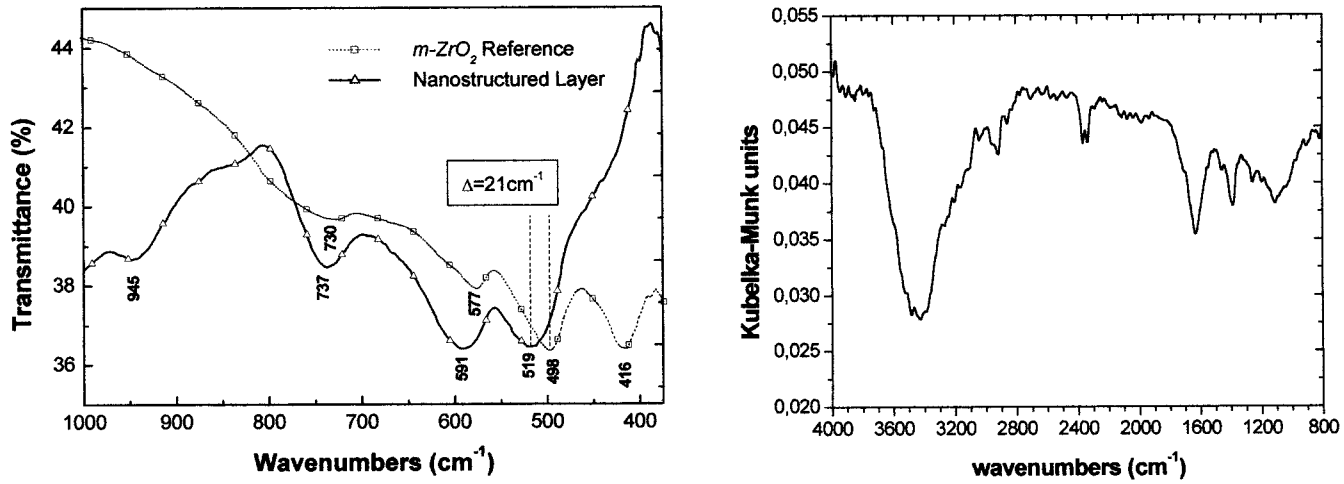

Figure 7. Infrared spectra of the nanostructured layer in the transmission mode (left), and in the DRIFTS mode (right).

at 730 cm^{-1}. Comparison with a zirconia spectrum obtained by sol−gel shows an important blue shift of the 498 and 577 cm^{-1} bands, whereas the 730 cm^{-1} band is more intense in sol−gel zirconia. The DRIFTS spectrum (Figure 7b) in the 4000−1200 cm^{-1} range in air shows a strong absorption band at about 3450 cm^{-1}, and additional bands at low frequencies in the 1600 and 1100 cm^{-1} regions.

Specific surface measurements were carried out on the powder resulting from oxidation after one month. The results are very sensitive to powder treatment before BET analysis: $S_{BET} = 21.0$ m^2/g and $S_{BET} = 25.7$ m^2/g are obtained after drying at 40 and 110 °C, respectively. Assuming that all the powder is transformed into gold and zirconia, the equivalent spherical agglomerate diameter is about 27 nm.

Discussion

Metallic ingots are stable in argon atmosphere or in a vacuum. Oxidation occurs very rapidly in air at room temperature. The novel mechanism of this nanostructuring oxidation is complex and cannot be described through a classical corrosion model. Indeed, the Pilling−Bedworth ratio Δ for ZrAu is about 1.35 (similar to that of aluminum, 1.38), and we should expect the formation of a thin protective film described by parabolic law followed by an asymptotic tendency. Nevertheless, the continuous formation over time of the nanostructured layer at the sample surfaces can be described by a linear law as follows:

$$d_{\text{layer}} = kt$$

where d_{layer} is the thickness of the layer, t is time, and k is a constant depending on the oxidation conditions ($k = 170$ nm·h^{-1} in air with 65% RH at 25 °C) and is very sensitive to the conditions in which initial intermetallic ingots are developed. The oxidation kinetics of ZrAu does not depend on the nanostructured layer thickness. The reaction products are gold and zirconia clusters showing increasing sizes over time at room temperature. Water pressure has been shown to accelerate this transformation drastically. Conversely, experiments in pure O_2 show that no oxidation was observed after one month at the observation scale of the electron microscope.

The IR absorption band of adsorbed molecular dioxygen on oxide surfaces is characterized by the ν_{O-O} doublet vibration centered at 1610 cm^{-1} for $[O_2]_{ads}$ at 20 °C on TiO_2 and 1605 cm^{-1} for $[O_2]_{ads}$ at 20 °C on SnO_2. The first step involves the dissociative adsorption of dioxygen and/or water molecules followed by its reduction toward forming oxide ions whereas zirconium is oxidized. This is consistent with DRIFT measurements showing a strong absorption band at 1619 cm^{-1}. The formation of Zr−oxygen groups on the zirconia surface is equivalent to the appearance of oxygen ions adsorbed on zirconium cations. The broad and poorly resolved band observed at about 1100 cm^{-1} could be related to the radical ion π-O_2^- form which appears in the 1040−1190 cm^{-1} range for both TiO_2 and SnO_2. The presence of peroxide radical O_2^{2-} is not observed in the DRIFT spectra.

The relative humidity sharply increases the oxidation rate. This rate is multiplied by 2 when RH varies from 65% to 100% at 25 °C. However, oxidation of ZrAu alloys in pure boiled water under argon atmosphere is strongly reduced, as is the case in many other alloys. The combination of −OH groups and oxygen molecules accelerates oxidation by forming an intermediate zirconium hydroxide. The large absorption band at 3450 cm^{-1} in the DRIFTS spectrum confirms the formation of hydroxyl groups at the surface of the alloy. However, an amorphous layer is not observed by HREM, indicating that this layer is very thin and/or only made of adsorbed −OH groups. Capillary condensation of water and pore filling are also expected for these surface areas.

In the case of pure zirconium, oxidation involves the movement of oxide ions inward through the film toward the metal. The large oxygen solubility (approximately 30 atom % at 25 °C) leads to the formation of a ZrO_x layer on the surface which turns into ZrO_2(t) and then ZrO_2(m). However, in the gold-containing zirconium alloy, the movement of oxide ions through the surface should be associated with the segregation of gold atoms out of the ZrO_x area formed during the first step. Indeed, Au−ZrO_2 solid solution has never been observed and is unlikely.

$$\text{ZrAu} + (x/2)\text{O}_2\,(\text{adsorbed}) \rightarrow \text{ZrO}_x + \text{Au (clusters)}$$

The second hypothesis could be the segregation of zirconium out of the ZrAu intermetallic phase toward

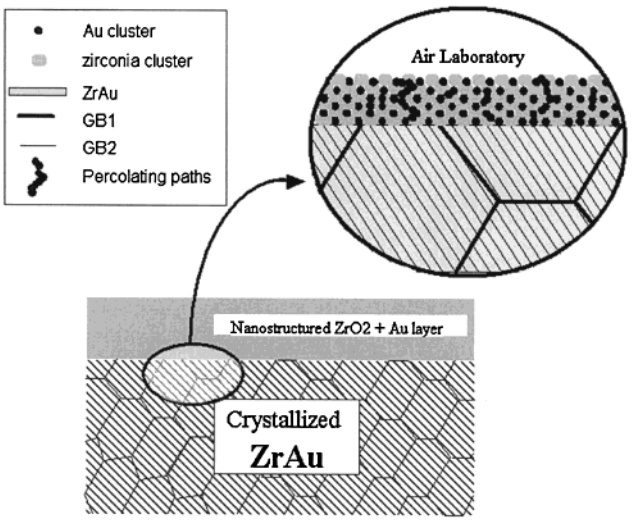

Figure 8. Schematic representation of cross-sections of ZrAu samples exposed to an air laboratory for 1 day.

the oxygen-rich region associated with the decrease of the Zr:Au ratio. However, XRD experiments did not reveal the formation of any additional Au-rich intermetallic compound. Fourier transforms of high-resolution images of gold clusters show, in small areas, additional spots that could be interpreted as a superstructure. Further investigations on this hypothesis are in progress.

Electron transfer from zirconium to adsorbed oxygen through the passivation layer is very low at room temperature for pure zirconium alloy due to the insulator properties of its oxides. Unlike pure zirconium, this layer is an insulator−metal nanocomposite with electronic conduction depending on the volume fraction of gold and topological parameters. When the transformation of ZrAu into Au and ZrO_2 is completed, the theoretical volume fraction of gold clusters in this layer is about $\Phi_{layer}[Au] = 0.33$. This value is higher than the percolation threshold of the fcc compact network of conducting particles (equal to 0.19) and near the percolation threshold deduced from the Monte Carlo simulation[11] equal to 0.31 for a three-dimensional bcc network. The percolation threshold of the electronic current through the nanostructured layer enhances the oxidation process (Figure 8). This mechanism could also explain why Zr_3Au with theoretical $\Phi_{layer}[Au]$ equal to 0.14 is stable in air at room temperature whereas Zr_2Au with $\Phi_{layer}[Au] = 0.20$ oxidizes in the same conditions. These observations are consistent with results obtained by Kimura et al. with amorphous Zr_xAu_y in which an increase of the noble metal content favors high-temperature oxidation.

The presence of large amounts of water molecules in air accelerates the nanostructuring oxidation by increasing the ionic conductivity, mainly on the surface of the zirconia particles. X-ray diffractograms of the nanostructured layer do not clearly show the most intense peaks of ZrO_2(t) expected for very small particles.[12] Asami et al. has also observed that water accelerates the structural transformation of very small zirconia clusters from metastable tetragonal to monoclinic zirconia in the oxidation of $Zr_{40}Cu_{60}$.[13]

The nanostructuring oxidation of crystallized ZrAu alloy observed at room temperature could be compared with an operating electrochemical cell continuously formed during the oxidation process (due to the overpotential induced by the strong difference in electrochemical potentials between dioxygen and zirconium).

anode: $ZrAu + 4OH^- \rightarrow ZrO(OH)_2 + H_2O + Au + 4e^-$

electrolyte: ZrO_x with a −OH group on the surface

external circuit: percolating network of Au clusters

cathode: $O_2(g) + 2H_2O + 4e^- \rightarrow 4OH^-$

This mechanism cannot explain the huge difference in the oxidation rates at the same composition between crystallized ZrAu (a few hours) and amorphous ZrAu (a few years). Additional effects are necessary to explain this unexpected chemical reactivity.

(1) Ultrafast Reactive Diffusion of Oxygen. As we mentioned in a previous work,[7] the morphology of the ZrAu phase may be understood as a double microstructure organization. The first type of grain boundary, noted GB1, results from the crystallization of large grains (100 μm) in accordance with the congruent formation of the equiatomic compound. The second type, noted GB2, characteristic of the transformation in the solid state (probably martensitic) generates smaller grains (100 nm) aligned in the same direction and related to important residual stress contained in ZrAu samples. Indeed, during cutting, sub-millimeter-size slices bend strongly to acquire a cylinder-like aspect. The rapid oxidation observed at 25 °C is probably exacerbated by internal residual stress associated with a martensitic-type transformation. Indeed, GB2 could accelerate species diffusion at room temperature, whereas internal stress is minimized by increasing the solid−gas interface area. These oriented structure defects, usually considered as preferential nucleation sites for segregation of atoms, could explain the resulting aligned roughness observed on the nanostructured layer (Figure 5b,c).

The hypothesis of the presence of at least two crystallographic forms of ZrAu could be supported by the two different oxidation kinetics observed for the intensity decreases of the diffraction peaks (categories A and B). One of these two phases is necessarily metastable, and its solid-state transformation occurring at the interface could induce ultrafast reactive diffusion of oxygen assisted by the collective displacement of Zr and Au atoms during this relaxation.

(2) Autocatalytic Nanostructuring Reaction. Very small gold nanoparticles deposited on selected metal oxides exhibit unusual catalytic activity in oxidation reactions at low temperature.[14−16] A. Cros et al.[17] have

(11) Ziff, R. M.; Stell, G. *Physical Review Letters LaSC* (*Ann Harbor, Michigan*); Report No. 88-4, 1988.
(12) Chraska, T.; King, A. H.; Berndt, C. C. *Mater. Sci. Eng., A* **2000**, *286*, 169−178.
(13) Asami, K.; Kikuchi, M.; Hashimoto, K. *Corros. Sci.* **1997**, *39*, 95−106.
(14) Valden, M.; Lai, X.; Goodman, D. W. *Science* **1998**, *281*, 1647.
(15) Grunwaldt, J. D.; Maciejewski, M.; Becker, O. S.; Fabrizioli, P.; Baiker, A. *J. Catal.* **1999**, *186*, 458−469.
(16) Bollinger, M. A.; Vanice, M. A. *Appl. Catal. Environ.* **1996**, *8*, 417.

shown that predeposition of gold atoms on the Si(111) surfaces considerably enhances the silicon oxidation process due to the catalytic action of gold at low temperature (<400 °C) whereas gold atoms have no influence at higher temperature on the oxidation process. We generally consider that O_2 gas does not readily dissociatively adsorb on Au, but Bondzie et al.[18] have shown that the Au−O chemisorption bond strength on thin gold islands is greater than on thick gold islands and should promote dissociative O_2 adsorption, which they postulate as a critical step in oxidative catalysis over Au/TiO_2. In th ecrystallized ZrAu sample, ultrafast reactive diffusion of oxide ions is associated with segregation of gold atoms to form very small Au clusters. Their size is limited by the room temperature; consequently, they can interact with gaseous species by dissociative adsorption. This interaction increases the oxidation rate by decreasing the energy of this intermediate state of the cathodic reaction.

$$O_2(g)\ (air) \rightarrow O_2\ (adsorbed) \rightarrow \text{“}\bullet O-O\bullet\text{”}$$

$$O_2\ (adsorbed) + 4\ e^- \rightarrow 2O^{2-}(s)$$

This mechanism could be called “autocatalytic nanostructuring oxidation”.

(17) Cros, A.; Derrien, J.; Salvan, F. *Surf. Sci.* **1981**, *110*, 471−490.

(18) Bondzie, V. A.; Parker, S. C.; Campbell, C. T. *J. Vac. Sci. Technol., A* **1999**, *17* (4), 1717−1720.

Conclusion

This preliminary study has shown that small zirconia and gold clusters are obtained spontaneously within a few hours from oxidation of crystallized ZrAu at room temperature. This unexpected reactivity appears for the first time in ZrAu. The mechanism involves a topological feature (percolation of gold clusters through the nanostructured layer) and a microstructure feature (residual internal stress and grain boundary). An interpretation is proposed to explain the huge difference in the oxidation rate between amorphous and crystallized ZrAu alloys:

(1) ultrafast reactive diffusion of oxygen assisted by stress relaxation,

(2) autocatalytic nanostructuring reaction involving very small gold clusters.

We may expect that ultrafast nanostructuring oxidation will be observed soon in other combinations of intermetallic compounds.

Acknowledgment. We thank P. Bowen and R. Oesch of the Powder Technology Laboratory (EPFL) for BET measurements and P. Stadelmann for his assistance with the HREM observations at the CIME, Swiss Federal Institute of Technology.

CM011184Z